The Journal of Immunology

Anti–PD-1 Checkpoint Therapy Can Promote the Function and Survival of Regulatory T Cells

Sarah C. Vick, Oleg V. Kolupaev, Charles M. Perou and Jonathan S. Serody

J Immunol published online 4 October 2021
http://www.jimmunol.org/content/early/2021/10/04/jimmunol.2001334

Supplementary Material **http://www.jimmunol.org/content/suppl/2021/10/04/jimmunol.2001334.DCSupplemental**

The Journal of Immunology is published twice each month by
The American Association of Immunologists, Inc.,
1451 Rockville Pike, Suite 650, Rockville, MD 20852

Print ISSN: 0022-1767 Online ISSN: 1550-6606.

Published October 4, 2021, doi:10.4049/jimmunol.2001334

Anti–PD-1 Checkpoint Therapy Can Promote the Function and Survival of Regulatory T Cells

Sarah C. Vick,*,[1] Oleg V. Kolupaev,[†] Charles M. Perou,[†,‡] and Jonathan S. Serody*,[†]

We have previously shown in a model of claudin-low breast cancer that regulatory T cells (T_{regs}) are increased in the tumor microenvironment (TME) and express high levels of PD-1. In mouse models and patients with triple-negative breast cancer, it is postulated that one cause for the lack of activity of anti–PD-1 therapy is the activation of PD-1–expressing T_{regs} in the TME. We hypothesized that the expression of PD-1 on T_{regs} would lead to enhanced suppressive function of T_{regs} and worsen antitumor immunity during PD-1 blockade. To evaluate this, we isolated T_{regs} from claudin-low tumors and functionally evaluated them ex vivo. We compared transcriptional profiles of T_{regs} isolated from tumor-bearing mice with or without anti–PD-1 therapy using RNA sequencing. We found several genes associated with survival and proliferation pathways; for example, *Jun*, *Fos,* and *Bcl2* were significantly upregulated in T_{regs} exposed to anti–PD-1 treatment. Based on these data, we hypothesized that anti–PD-1 treatment on T_{regs} results in a prosurvival phenotype. Indeed, T_{regs} exposed to PD-1 blockade had significantly higher levels of Bcl-2 expression, and this led to increased protection from glucocorticoid-induced apoptosis. In addition, we found in vitro and in vivo that T_{regs} in the presence of anti–PD-1 proliferated more than control T_{regs}. PD-1 blockade significantly increased the suppressive activity of T_{regs} at biologically relevant T_{reg}/T_{naive} cell ratios. Altogether, we show that this immunotherapy blockade increases proliferation, protection from apoptosis, and suppressive capabilities of T_{regs}, thus leading to enhanced immunosuppression in the TME. ***The Journal of Immunology*****, 2021, 207: 1–10.**

Breast cancer is the most prevalent malignancy in women, accounting for 30% of newly diagnosed cancer cases (1). In 2021, more than 44,000 women and men in the United States are expected to die of breast cancer (2). The clinical prognosis of patients with breast cancer is dependent on tumor grade, involvement of lymph nodes, and expression of the hormone and growth factor receptors estrogen receptor progesterone receptor, and human epidermal growth factor receptor 2 (3). The triple-negative breast cancer (TNBC) subtype is characterized by the lack of expression of estrogen receptor, progesterone receptor, and human epidermal growth factor receptor 2. This clinical subtype can be further divided into molecular groups, including the basal-like and claudin-low subtypes, which include the majority of TNBC tumors (4, 5). The basal-like and claudin-low subtypes are defined by increased expression of tumor-proliferative genes and high infiltration of immune cells (6). TNBC has the worst prognosis of the breast cancer subtypes because of the lack of targeted therapies that define the other breast cancer subtypes. Because of this, surgery, radiation, and chemotherapy are first-line treatments for TNBC, but because of immune involvement, immunotherapeutic strategies to treat these types of tumor hold great promise.

Immunotherapy has been a promising new approach to cancer treatment in the last decade. Immunotherapy involves enhancing the patient's immune cells to kill tumor cells. PD-1/PD-L1 signaling is an important adaptive immune response pathway to ensure the immune system is activated only at the appropriate times to minimize inflammation in the setting of persistent Ag. PD-1 expression on T cells from patients with cancer is critical to the progressive dysfunction of these cells in the tumor microenvironment (TME) (7). Tumors can use this immune suppression mechanism by overexpressing PD-L1 (8), the ligand to the PD-1 receptor, thus dampening antitumor immune activity in the TME. Most of the previous studies evaluating the function of PD-1 have been focused on cytotoxic $CD8^+$ T cell function in the context of both chronic viral infections and cancer (9). $CD8^+$ T cell exhaustion is characterized by the loss of proliferation, reduction in proinflammatory cytokine production, and diminished cytotoxic activity (10). This loss of function can be reversed by blocking the PD-1/PD-L1 signaling axis, restoring cytokine production, proliferation, and leading to an enhanced immune response (11). The role of PD-1 on other types of immune cells in the TME is much less well understood.

*Department of Microbiology and Immunology, University of North Carolina, Chapel Hill, NC; [†]Lineberger Comprehensive Cancer Center, University of North Carolina, Chapel Hill, NC; and [‡]Department of Genetics, University of North Carolina, Chapel Hill, NC

[1]Current address: Department of Vaccine and Infectious Disease Division, Fred Hutchinson Cancer Research Center, Seattle, WA

ORCIDs: 0000-0002-0552-0078 (S.C.V.); 0000-0001-9827-2247 (C.M.P.); 0000-0003-4568-1092 (J.S.S.).

Received for publication November 24, 2020. Accepted for publication September 4, 2021.

This work was supported by grants from the following: National Institute of Allergy and Infectious Diseases (NIAID), University of North Carolina (UNC) Basic Immune Mechanisms (T32AI007273-33) to S.C.V., Breast Cancer Specialized Program of Research Excellence (P50 CA058223) to J.S.S. and C.M.P., National Heart Lung and Blood Institute (R01 HL139730) to J.S.S., and a Research Opportunities Initiative Grant from the State of North Carolina to J.S.S. The UNC Flow Cytometry Core Facility and High Throughput Sequencing Facility are supported in part by Cancer Center Support Grant P30 CA016086 to the UNC Lineberger Comprehensive Cancer Center.

S.C.V designed research studies, conducted experiments, analyzed data, and wrote the manuscript. O.V.K. performed experiments and edited the manuscript. C.M.P. provided reagents and edited the manuscript. J.S.S. designed research studies and wrote the manuscript.

Address correspondence and reprint requests to Dr. Jonathan S. Serody, Marsico Hall, 125 Mason Farm Road, CB7595, University of North Carolina, Chapel Hill, NC 27599. E-mail address: jonathan_serody@med.unc.edu

The online version of this article contains supplemental material.

Abbreviations used in this article: 7-AAD, 7-aminoactinomycin D; Dex, dexamethasone; GC, glucocorticoid; GITR, GC-induced TNF receptor; IPA, Ingenuity Pathway Analysis; MFI, mean fluorescence intensity; p_{adj}, p adjusted value; RNA-seq, RNA sequencing; TIL, tumor-infiltrating lymphocyte; TME, tumor microenvironment; T_{reg}, regulatory T cell.

Our group has previously shown that TNBC is typically heavily infiltrated with both adaptive and innate immune cells (12). Most recently, the IMPassion130 Study demonstrated a significant improvement in progression-free survival in patients treated with the anti–PD-L1 mAb atezolizumab plus nab-paclitaxel, a microtubule-disrupting chemotherapy agent, compared with those receiving the chemotherapy alone (13). Despite this, the clinical response for patients with TNBC treated with anti–PD-1 or PD-L1 mAb therapy alone was modest, with 6–19% of patients responding to therapy and with none of these patients responding persistently. In addition, in many cancers refractory to PD-1 blocking therapy, it has been reported that a subset of these patients can experience hyperprogression of cancer (14–16) from anti–PD-1 immunotherapy. The reason for this hyperprogression is not well understood, although it is noteworthy that regulatory T cells (T_{regs}) are increased after PD-1 blockade in these patients (14, 17, 18). Thus, although PD-1 expression on cytotoxic $CD8^+$ T cells may be the primary target of immune checkpoint inhibition, it is becoming evident that PD-1 expressed by other immune cell subsets could contribute significantly to the effectiveness of checkpoint blockade (19–22).

A major limitation to characterizing the function of PD-1 on non-$CD8^+$ T cells has been the lack of tumor models with substantial expression of PD-1 on immune cells other than $CD8^+$ tumor-infiltrating lymphocytes (TILs). Although it has been demonstrated in various tumor settings that T_{regs} often express high levels of PD-1, until now a suitable model for studying checkpoint blockade in tumors highly infiltrated with PD-1^+ T_{regs} was not feasible. Work from our group has shown that in a mouse model of claudin-low breast cancer, the frequency of $CD4^+$ $Foxp3^+$ T_{regs} expressing PD-1 was greater than the frequency of PD-1^+ $CD4^+$ conventional T cells and $CD8^+$ T cells subsets (23). Because T_{regs} provide an important mechanism of immune suppression and evasion in cancer progression (24), we used our previous model and two additional models to evaluate the hypothesis that PD-1^+ T_{regs} could be enhancing immune suppression in the TME after PD-1 blockade and potential mechanisms for this finding.

Materials and Methods

Mice and cell lines

BALB/cJ, BALB/c Foxp3-GFP, BALB/c Thy1.1, and C57BL/6J (B6) females were purchased from The Jackson Laboratory (Bar Harbor, ME). Female mice (8–14 wk) were used for all experiments. T11 and T12 (claudin-low) tumor models have been described (23, 25). T12 cells were prepared by harvesting a T12 tumor from a tumor-bearing mouse, followed by manual and chemical digestion to form a single-cell suspension. E0771 cells were obtained from American Type Culture Collection (ATCC). All tumor cells lines were found to be free of mycoplasma as determined by PCR testing. BALB/c mice were injected with 1×10^4 T11 (claudin-low) cells in PBS or 1×10^5 T12 (claudin-low) cells in Matrigel high concentration low-growth factor. B6 mice were injected with 2.5×10^5 E0771 (luminal) cells in PBS. Tumors were orthotopically transplanted by intradermal injection into a mammary fat pad and measured twice per week using calipers. Tumor width × height was recorded, and mice were sacrificed at the specified tumor size or at the Institutional Animal Care and Use Committee–approved end point of 2 cm^2.

Study approval

All animal experiments were conducted in accordance with protocols approved by the University of North Carolina Institutional Animal Care and Use Committee.

Isolation of murine TILs

Murine tumors were resected and digested in Liberase TL (5401020001; Roche), DNase I (D4527; Sigma), Hyaluronidase (Sigma), and Collagenase XI (C9697; Sigma), as previously described (26). Single-cell suspensions were enriched for lymphocytes by isolating cells at the interface of a 44% Percoll (P1644; Sigma) in media and Lympholyte-M (CL5031; Cedarlane) gradient.

Abs and flow cytometry reagents

Flow cytometry mAbs against murine CD45 (30-F11, #11-0451-82), Foxp3 (FJK-16S, #45-5773-82), PD-1 (J43, #48-9981-82), Ki67 (SolA15, #17-5698-80), Thy1.1 (HIS51, #45-0900-80), CTLA-4 (UC10-4B9, #12-1522-82), and GC-induced TNF receptor (GITR; DTA-1, #25-5874-82) were purchased from Invitrogen. mAbs against murine CD4 (GK1.5, #100414), CD8 (53-6.7, #100722), PD-1 (RMP1-30, #109103), LAP-TGF-β (TW7-16B4, #141405), CD25 (PC61, #102051), and BrdU (Bu20a, #339808) were purchased from BioLegend. mAbs against murine Bcl-2 (3F11, #556537) were purchased from BD Biosciences (San Jose, CA), and mAbs against murine Bim (C34C5, #948055) were purchased from Cell Signaling Technology. Cell viability was determined using Aqua Fluorescence Reactive Dye (#L34965; Life Technologies). For flow cytometry, cells were surface stained and fixed/permeabilized overnight using the Foxp3/Transcription Factor Staining Buffer Set (#00-5523-00; eBioscience), and intracellular staining was performed the following day according to the manufacturer's instructions. Apoptosis was measured using PE Annexin V Apoptosis Detection Kit (#559763; BD Pharmingen). Data were acquired using the BD FACSCanto or BD LSRFortessa (BD Biosciences). Acquired data were analyzed using FlowJo Flow Cytometry Analysis Software (FlowJo, Ashland, OR).

Proliferation assays using BrdU incorporation

Tumor-bearing BALB/c mice were injected with 2 mg BrdU i.p. in 200 μl DPBS 24 h before TIL isolation. Isolated TILs were stained using allophycocyanin BrdU Flow Kit (51-9000019AK; BD Biosciences) adapting the manufacturer's protocol. In brief, cells were stained for surface Ags, then resuspended in BD Cytofix/Cytoperm buffer for 30 min on ice. Cells were washed with Perm/Wash and resuspended in BD Cytoperm Permeabilization Buffer Plus for 10 min on ice. Cells were then refixed/permeabilized overnight using the Foxp3/Transcription Factor Staining Buffer Set (00-5523-00; eBioscience). Cells were then treated with 30 μg DNase for 1 h at 37°C. Cells were then stained for intracellular proteins including BrdU for 30 min at room temperature. Data were acquired using the BD FACSCanto (BD Biosciences). Acquired data were analyzed using FlowJo Flow Cytometry Analysis Software.

In vivo Abs

mAbs used for in vivo Ab inhibition were purchased from BioXCell (#BE0033-2). Mice undergoing immune checkpoint inhibition received i.p. injection of 200 μg anti–PD-1 (J43) or 200 μg anti–PD-1 (J43) Ag binding fragments (Fabs) created using Pierce Fab Preparation Kit (44985; Thermo Fisher) on day +7 posttumor implantation when the tumor was palpable and then every 3–4 d throughout the experiment.

RNA sequencing

$Foxp3^+$ GFP^+ T_{regs} isolated from tumors were sorted using a MoFlo XDP (Backman Coulter, Pasadena, CA) to >90% purity. RNA was isolated from sorted T_{regs} using RNeasy Micro Kit (Qiagen, Germantown, MD). RNA sequencing (RNA-seq) libraries were constructed with NuGEN Ovation SoLo (NuGEN Technologies, Redwood City, CA). Samples were sequenced using Illumina HiSeq 2500 Rapid Run (Illumina, San Diego, CA). Differential gene expression analysis was performed using DESeq2 (27). Ingenuity Pathway Analysis (IPA) was performed in a Web portal (https://www.qiagenbioinformatics.com/products/ingenuity-pathway-analysis/).

T_{reg} suppression and proliferation assays

For the T_{reg} suppression assays, we evaluated tumor-infiltrating T_{regs}. $Foxp3^+GFP^+$ cells were sorted from tumors of T11 (claudin-low)-bearing mice using a MoFlo XDP (Beckman Coulter, Pasadena, CA) or FACSAria II (BD Biosciences) cell sorter to >90% purity. APCs were isolated from wild-type BALB/cJ splenocytes after CD90 microbead depletion (130-049-101; Miltenyi) and irradiation at 30 Gy. Responder cells were isolated from BALB/c Thy1.1 mice using a T recovery column kit (CL101; Cedarlane). Isolated cells were then B220 and CD25 depleted using PE-conjugated Abs and anti-PE magnetic bead sorting (130-048-801; Miltenyi). Responder cells were stained with the Cell Proliferation Dye eFluor 670 (65-0840; eBioscience) and plated at varying T_{reg}/effector T cell ratios with soluble anti-CD3 (16-0031-85; eBioscience). Cells were cocultured for 3 d, stained, and FACS analyzed.

For the assays measuring proliferation of T_{regs} ex vivo, we evaluated tumor-infiltrating T_{regs}. $Foxp3^+$ GFP^+ cells were sorted on a cell sorter similar to described earlier to >90% purity. The sorted T_{regs} were then stained with the Cell Proliferation Dye eFluor670 (65-0840; eBioscience) and plated

with irradiated APCs and soluble anti-CD3 with or without anti–PD-1 Fabs in the cell culture. Fabs of PD-1 made from Ab clone J43 were used in vitro cultures to eliminate effects from Fc-mediated activity of the Abs. Cells were cultured for 3 d, stained, and FACS analyzed.

T_{reg} apoptosis assays

For the assays measuring ex vivo T_{reg} apoptosis, we evaluated tumor-infiltrating T_{regs}. After isolation of TILs, the isolated lymphocytes were enriched for total T cells using a T recovery column kit (CL101; Cedarlane). T cells were then cultured with 10 μM dexamethasone (Dex; D4902; Sigma) for 24 h with or without anti–PD-1 Fabs (BE0033-2; BioXCell) in the cell culture. Cells were then harvested, stained with PE Annexin V Apoptosis Detection Kit (559763; BD Pharmingen), and FACS analyzed.

Bcl-2 inhibition in vivo

Bcl-2 inhibition was accomplished using Venetoclax (ABT-199). ABT-199 was purchased from MedChemExpress (HY-15531). ABT-199 was formulated in a mixture of 60% Phosal 50 PG (NC0130871; Fisher), 30% PEG 400 (202398-5G; Sigma), and 10% ethanol (BP2818-500; Fisher). Mice were dosed with ABT-199 or vehicle alone in 0.2 mL at 100 mg/kg/day by oral gavage. Mice were treated starting at day 3 after tumor injection and daily for the duration of tumor growth.

MTT assay with ABT-199

T11 cells were plated in a 96-well plate in complete media and incubated overnight. Venetoclax (ABT-199) was dissolved in DMSO, diluted in complete media, and added to the T11 cells at a starting concentration of 20 μM. T11 cells with ABT-199 were incubated at 37°C, 5% CO_2 for 48 h. Cells were then harvested, and cell death was determined using MTT Cell Growth Assay (CGD1; Sigma) following the manufacturer's protocols. ABT-199 dose–response curve and IC_{50} were calculated using Prism (GraphPad, San Diego, CA).

Results

In our model of claudin-low breast cancer, a large number of T_{regs} infiltrating the tumor expressed PD-1. The level of PD-1 expression on T_{regs} was not uniform (Fig. 1A), with the majority of PD-1^+ T_{regs} expressing low levels of the protein, while some T_{regs} expressed higher levels of PD-1 (Fig. 1B). Although fewer in proportion, the PD-1^{hi} T_{reg} population had a significant increase in suppressive molecules, such as CTLA-4 ($p = 0.05$) and proteins critical to T_{reg} function, such as the high-affinity IL-2 receptor α subunit, CD25 ($p = 0.028$) (Fig. 1C).

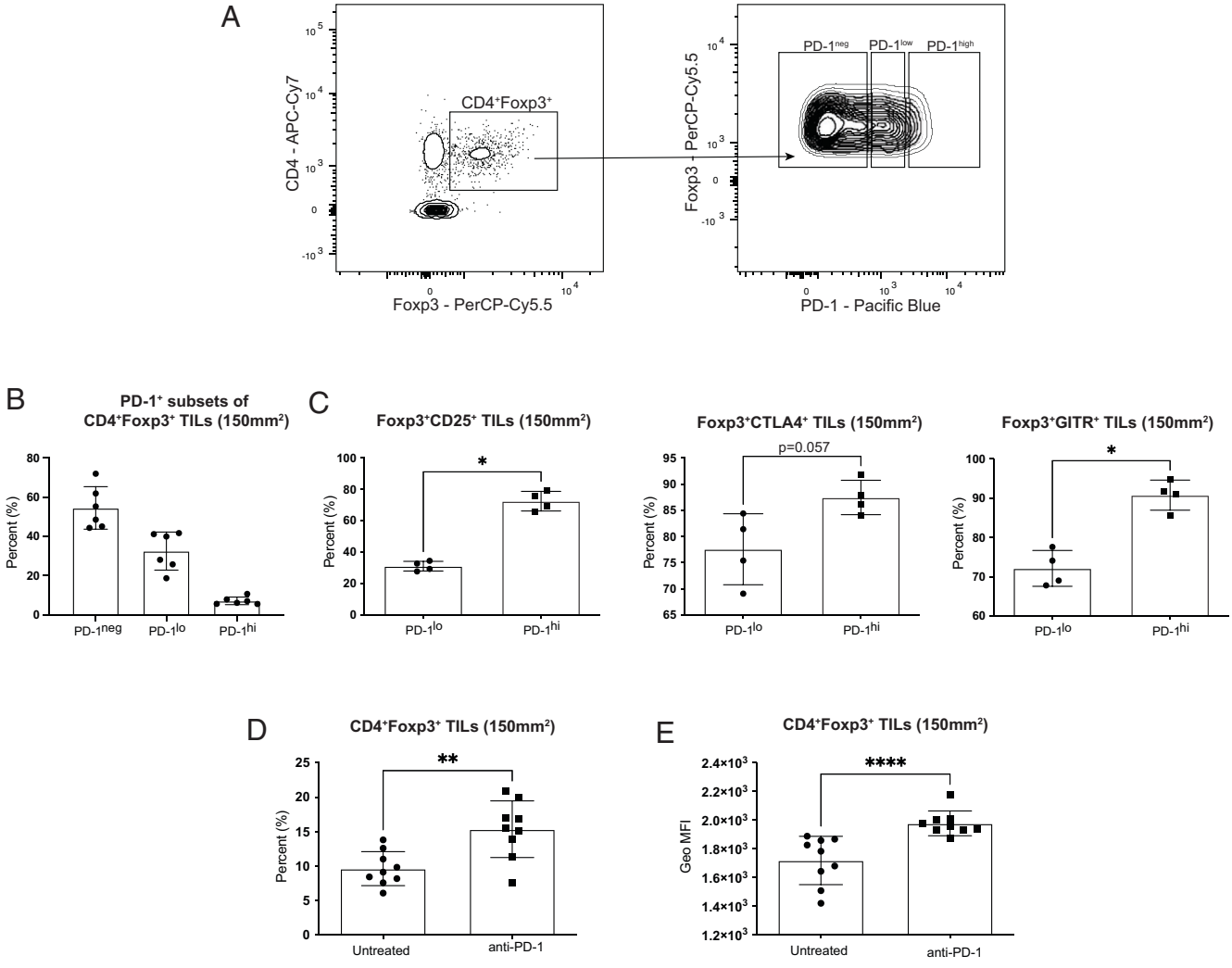

FIGURE 1. Infiltrating T_{regs} increase in the tumor after PD-1 blockade. Mice were injected with 1×10^4 T11 (claudin-low) tumor cells. Tumors were harvested at 150 mm^2, digested, enriched for lymphocytes, and analyzed by FACS. Cells were gated on lymphocytes/single cells/live/$CD3^+$/$CD4^+Foxp3^+$ and then analyzed for T_{reg} markers. (**A**) Representative flow plots gated on $CD4^+Foxp3^+$ T_{regs} showing PD-1 expression levels. (**B**) Percent PD-1^{neg}, PD-1^{lo}, and PD-1^{hi} $CD4^+Foxp3^+$ T_{regs} ($n = 6$). (**C**) Percent $CD4^+Foxp3^+$ T_{regs} expressing CD25 or CTLA-4 in PD-1^{lo} versus PD-1^{hi} populations ($n = 4$). (**D** and **E**) Mice were untreated or treated with 200 μg anti–PD-1 Ab (J43) injected i.p. twice a week for the duration of the experiment. (D) Percent $CD4^+Foxp3^+$ T_{regs} from the $CD45^+$ gated population ($n = 9$). (E) Geometric (Geo) MFI of Foxp3 in $CD4^+Foxp3^+$ cells ($n = 9$). Statistical significance was determined by Mann–Whitney *U* test. *$p < 0.05$, **$p < 0.01$, ****$p < 0.0001$.

Although the functional differences between these PD-1$^+$ T_{reg} populations are unknown, it has been shown that only intermediate PD-1–expressing CD8$^+$ T cells can be rescued by PD-1 blockade, while PD-1^{high} T cells are committed to exhaustion (28). Because we observed a low percentage of PD-1^{high}–expressing cells, we assessed the outcome of PD-1 blockade on the PD-1$^+$ T_{regs} infiltrating the claudin-low tumors. We compared CD4$^+$Foxp3$^+$ TILs from untreated mice with mice treated with anti–PD-1 Ab and saw a significant increase in the frequency of T_{regs} in mice treated with PD-1 blockade ($p = 0.004$) (Fig. 1D). We also observed a significant increase in Foxp3 levels measured by the geometric mean fluorescence intensity (MFI) of Foxp3 in T_{regs} treated with PD-1 blockade ($p < 0.001$) (Fig. 1E). Higher Foxp3 levels have been directly associated with increased suppressive capabilities in T_{regs} (29), thereby suggesting that T_{regs} treated with PD-1 blockade could lead to increased immunosuppression in the TME in claudin-low tumors.

To determine whether there were transcriptional differences between T_{regs} isolated from untreated claudin-low tumors versus T_{regs} from tumors treated with PD-1 blockade, we sorted GFP$^+$ T_{regs} from Foxp3^{GFP} reporter mice and performed RNA-seq. This demonstrated transcriptional changes in the T_{regs} from tumors treated with PD-1 blockade (Fig. 2A). We found 27 significantly differentially regulated genes in T_{regs} isolated from mice treated with PD-1 blockade when compared with untreated controls (p adjusted value [p_{adj}] < 0.05) (Table I). We used IPA to determine whether any biological pathways were affected by PD-1 blockade in our RNA-seq data. IPA predicted that the apoptosis pathway was inhibited when T_{regs} were treated with PD-1 blockade. In addition, *Jun* and *Fos* ($p = 0.001$), genes responsible for T cell proliferation (30), were significantly upregulated in T_{regs} from tumors treated with PD-1 blockade (Fig. 2B). Bcl-2, an antiapoptotic protein, was also significantly upregulated ($p = 0.028$) in T_{regs} isolated from tumors treated with PD-1 blockade (Fig. 2B). Based on these data, we hypothesized that PD-1 blockade in claudin-low tumors was promoting a prosurvival phenotype in T_{regs}.

To test this hypothesis, we first evaluated the proliferative potential of T_{regs} in vitro. T_{regs} cultured with anti–PD-1 Fabs proliferated significantly more than T_{regs} without anti–PD-1 in the culture ($p < 0.0001$) (Fig. 3A, 3B). To confirm that the significant proliferation of T_{regs} resulted from activation through CD3/CD28 engagement rather than an artifact of the anti–PD-1 Fabs, we cultured T_{regs} with anti–PD-1 Fabs alone without anti-CD3. PD-1 blockade alone did not lead to T_{reg} proliferation (Supplemental Fig. 1), suggesting that the increase in proliferation is due to the release of the inhibitory signal from PD-1, thus allowing the T_{regs} to proliferate. We next investigated whether the increase in T_{reg} proliferation was also present in vivo in the TME. To address this question, we evaluated cellular proliferation by BrdU incorporation. When immune cells were

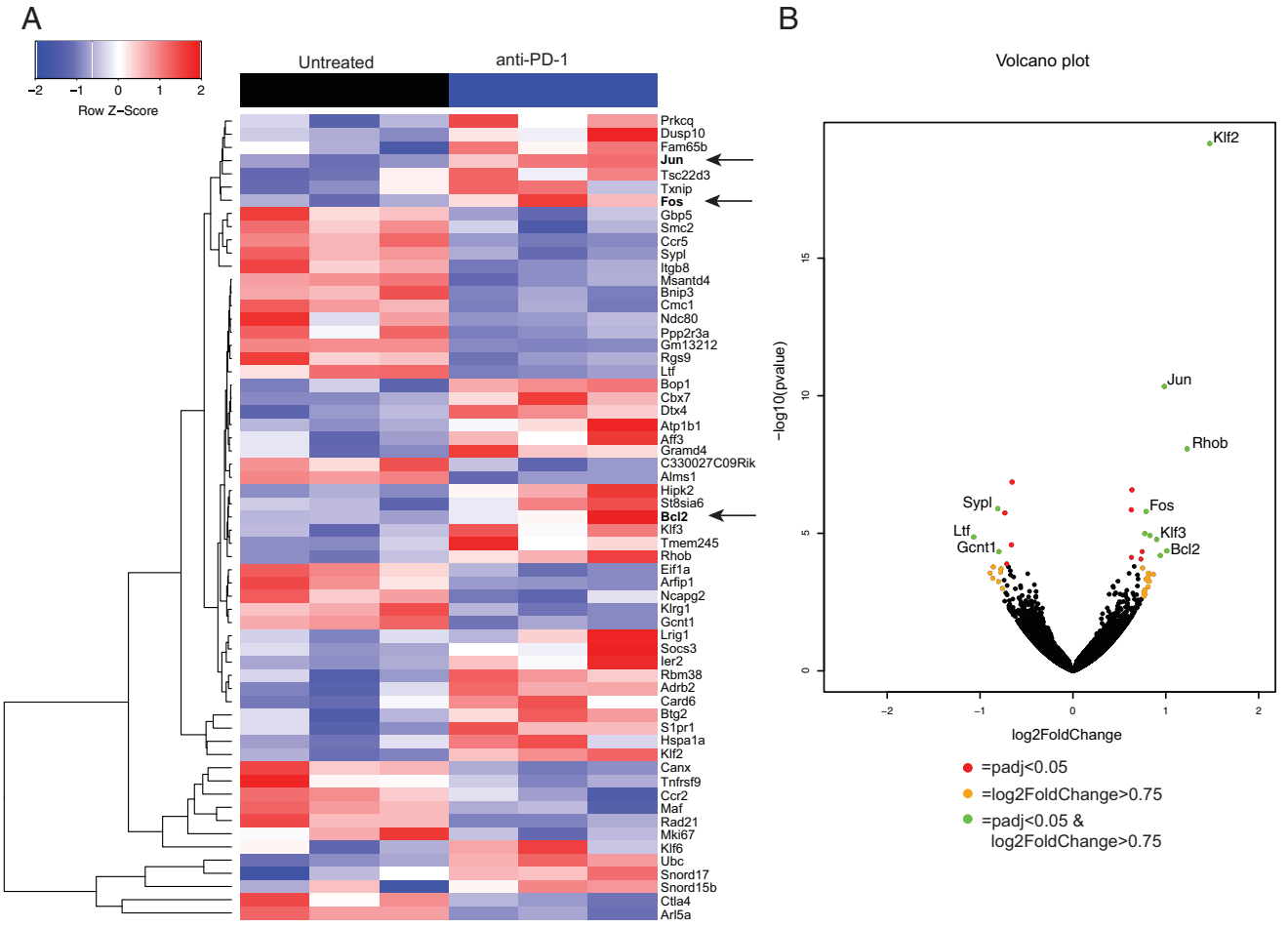

FIGURE 2. T_{reg} transcriptional profile changes with PD-1 blockade compared with untreated. Foxp3-GFP mice were injected with 1×10^4 T11 (claudin-low) cells and were untreated or treated with 200 μg anti–PD-1 Ab (J43) injected i.p. twice a week. Tumors were harvested at 150 mm^2, digested, and enriched for lymphocytes, and GFP$^+$ T_{regs} were sorted to >90% purity using MoFlo XDP cell sorter. RNA was isolated from sorted cells, and RNA-seq was performed on the HiSeq 2500 Rapid Run platform ($n = 6$). (**A**) Samples were clustered using hierarchal clustering. Z score of raw counts normalized among samples within each group. (**B**) Volcano plot showing significantly differentially regulated genes with $p_{adj} < 0.05$ and $\log_2$ fold change > 0.75.

Table I. Genes significantly regulated in T_{regs} treated with PD-1 blockade versus untreated

Gene	Base Mean	Log_2 Fold Change	p_{adj}
Upregulated			
Klf2	1351.561	1.473	5.55E−16
Jun	1034.796	0.984	1.86E−07
Rhob	300.810	1.230	2.31E−05
Ubc	5773.062	0.635	0.0004
S1pr1	1512.735	0.629	0.0016
Fos	809.493	0.788	0.0016
Ier2	646.815	0.774	0.0083
Adrb2	328.347	0.830	0.0088
Klf3	254.169	0.903	0.0104
Atp1b1	72.096	1.011	0.0221
Tsc22d3	942.382	0.746	0.0221
Bcl2	203.146	0.940	0.0288
Snord17	5426.186	0.630	0.0319
Card6	481.202	0.731	0.0350
Downregulated			
Arl5a	5260.143	−0.655	0.0003
Sypl	553.684	−0.809	0.0016
Ccr5	652.223	−0.732	0.0016
Ltf	48.023	−1.069	0.0092
Itgb8	972.937	−0.662	0.0152
Gcnt1	300.171	−0.797	0.0220
Klrg1	370.393	−0.712	0.0499

Foxp3-GFP mice were injected with 1×10^4 T11 (claudin-low) cells and were untreated or treated with 200 μg anti–PD-1 Ab (J43) injected i.p. twice a week. Tumors were harvested at 150 mm^2, digested, and enriched for lymphocytes, and GFP^+ T_{regs} were sorted to >90% purity using MoFlo XDP cell sorter. RNA was isolated from sorted cells, and RNA-seq was performed on the HiSeq 2500 Rapid Run platform ($n = 6$). Differential gene expression analysis was performed using DESeq2. Genes listed are significantly upregulated or downregulated with $p_{adj} < 0.5$.

isolated early during tumor growth (tumor size of 50 mm^2), the T_{regs} proliferated significantly more than $CD8^+$ or $CD4^+Foxp3^-$ T cells ($p = 0.029$) (Fig. 3C). We could not detect a difference in proliferation between T_{regs} from mice treated with anti–PD-1 versus untreated (data not shown) on day 15 after tumor injection (50 mm^2). We then evaluated proliferation at day 23 after tumor injection, by measuring expression of proliferation marker Ki-67 (31). We saw a nonsignificant increase in the frequency and total number of proliferating T_{regs} from mice treated with anti–PD-1 Fabs compared with untreated mice (Fig. 3D, 3E). We have previously published in this model of claudin-low breast cancer that T_{regs} infiltrating into the tumors have significantly higher levels of PD-1 expression than $CD8^+$ T cells (23). We predicted that PD-1 blockade would have a reduced impact on $CD8^+$ T cells than it does on T_{regs} because of the reduced PD-1 expression. Indeed, PD-1 blockade did not increase the frequency of $CD8^+Ki67^+$ T cells compared with untreated mice (Fig. 3F). T_{regs} not only have increased proliferation when exposed to anti–PD-1, but in our model of claudin-low breast cancer, the T_{regs} proliferate at a higher rate than other T cell subsets (Fig. 3C), suggesting an increased potential for T_{reg}-mediated suppression in the TME.

From our RNA-seq data, we found that *Bcl-2* was significantly upregulated in T_{regs} during treatment with anti–PD-1 (Fig. 2B). As an antiapoptotic protein, Bcl-2 expression can protect cells from apoptosis induced by various stimuli (32). To validate our RNA-seq data, we confirmed that Bcl-2 protein was upregulated in T_{regs} isolated from tumors treated with anti–PD-1. Mice were injected with claudin-low tumors, treated with anti–PD-1, or left untreated, and then tumors were harvested at 150 mm^2 to analyze protein expression by flow cytometry. The frequency of $Bcl\text{-}2^+CD4^+Foxp3^+$ cells was approximately eight times higher in T_{regs} from anti–PD-1 treated mice when compared with untreated mice (Fig. 4A, 4B). Mice treated with anti–PD-1 also had a significant increase in the levels of Bcl-2 in T_{regs} when compared with T_{regs} from untreated mice ($p = 0.018$) (Fig. 4D). We also measured the proapoptotic protein Bim and saw no difference in Bim frequency or expression levels between the two treatment groups of T_{regs} (Fig. 4C, 4E). Bcl-2/Bim ratios are often used as a measure for survival potential in cells. T_{regs} exposed to anti–PD-1 had significantly higher Bcl-2/Bim ratios than untreated T_{regs} ($p = 0.028$) (Fig. 4F), suggesting a potential for increased protection of T_{regs} from apoptosis in the TME. Thus, both the increased frequency of $Bcl\text{-}2^+$ T_{regs} and the increased expression of Bcl-2 in T_{regs} could enhance resistance of T_{regs} to apoptosis on treatment with anti–PD-1 mAb therapy.

Because we found a significant increase in levels of Bcl-2 in the T_{regs} from T11 (claudin-low) tumors (Fig. 4A), we sought to test whether these T_{regs} were protected from apoptosis ex vivo. Antiapoptotic Bcl-2 expression has been shown to inhibit glucocorticoid (GC)-induced apoptosis, so we tested whether Bcl-2 expressed in T_{regs} could protect them from Dex-induced apoptosis. Tumor-infiltrating T cells were isolated from control Foxp3-GFP T11 (claudin-low) tumor-bearing mice, as well as from mice treated with anti–PD-1 twice weekly, and then cultured ex vivo with or without Dex. Apoptosis in T_{regs} was assessed using Annexin V/7-aminoactinomycin D (7-AAD) staining. There was greater protection from apoptosis in T_{regs} from mice treated with anti–PD-1 and cultured in Dex than T_{regs} from untreated mice ($p < 0.0001$) (Fig. 5A, 5B). Interestingly, we did not see this significant decrease in cell death in $CD8^+$ T cells from mice treated with anti–PD-1 (Fig. 5C), suggesting that this protection from apoptosis may be specific to T_{regs} in the TME. We confirmed our findings in an additional model of claudin-low breast cancer (T12). There was a decrease in T_{regs} undergoing apoptosis when treated with PD-1 blockade, and this decrease was sustained with the addition of Dex (Supplemental Fig. 2A). To determine whether this protection from apoptosis could be attributed to Bcl-2, we added Venetoclax (ABT-199), a potent and selective Bcl-2 inhibitor. When Bcl-2 was inhibited in vitro, there was no longer a reduction in T_{regs} undergoing apoptosis with PD-1 blockade (Supplemental Fig. 2A). To determine whether this protection from apoptosis after PD-1 blockade was specific to claudin-low breast cancer, we employed a model of luminal breast cancer (E0771). We determined that unlike the T11 and T12 claudin-low models of breast cancer where there is a greater frequency of T_{regs} than $CD8^+$ T cells expressing PD-1, the E0771 model of breast cancer had a higher frequency of $CD8^+$ T cells that were $PD\text{-}1^+$ (Supplemental Fig. 2B). When we assessed apoptosis in T_{regs} in mice with E0771 tumors, these cells were not protected from apoptosis induced by Dex (Supplemental Fig. 2C, 2D). Interestingly, $CD8^+$ T cells from mice treated with PD-1 blockade were protected from apoptosis in the E0771 luminal breast cancer model (Supplemental Fig. 2E). Thus, protection from apoptosis was directly correlated with the difference in the expression of PD-1 by T_{regs} and $CD8^+$ T cells.

We also treated mice with a Bcl-2 inhibitor to determine whether there would be increased apoptosis in T_{regs}. Mice treated with Bcl-2 inhibitor ABT-199 had delayed tumor growth and increased survival irrespective of anti–PD-1 treatment (Supplemental Fig. 3A, 3B). Although it is possible that ABT-199 had a direct effect on the T11 tumor cells themselves, the EC_{50} against T11 cells in vitro was 2 μM (Supplemental Fig. 3D), while the IC_{50} of ABT-199 on Bcl-2–expressing hematopoietic cells is 4 nM (33), suggesting that in our system ABT-199 does not have potent activity against T11 (claudin-low) tumor cells and is likely acting by inhibiting T_{reg} function. However, ABT-199 therapy did not enhance the efficacy of anti–PD-1 mAb in this model. Although the total number of T_{regs} infiltrating into the tumor after treatment with ABT-199 was similar, the number of $CD8^+$ T cells was significantly decreased (Supplemental Fig. 3C), indicating that the effect of Bcl-2 inhibition on the presence of T cells in the

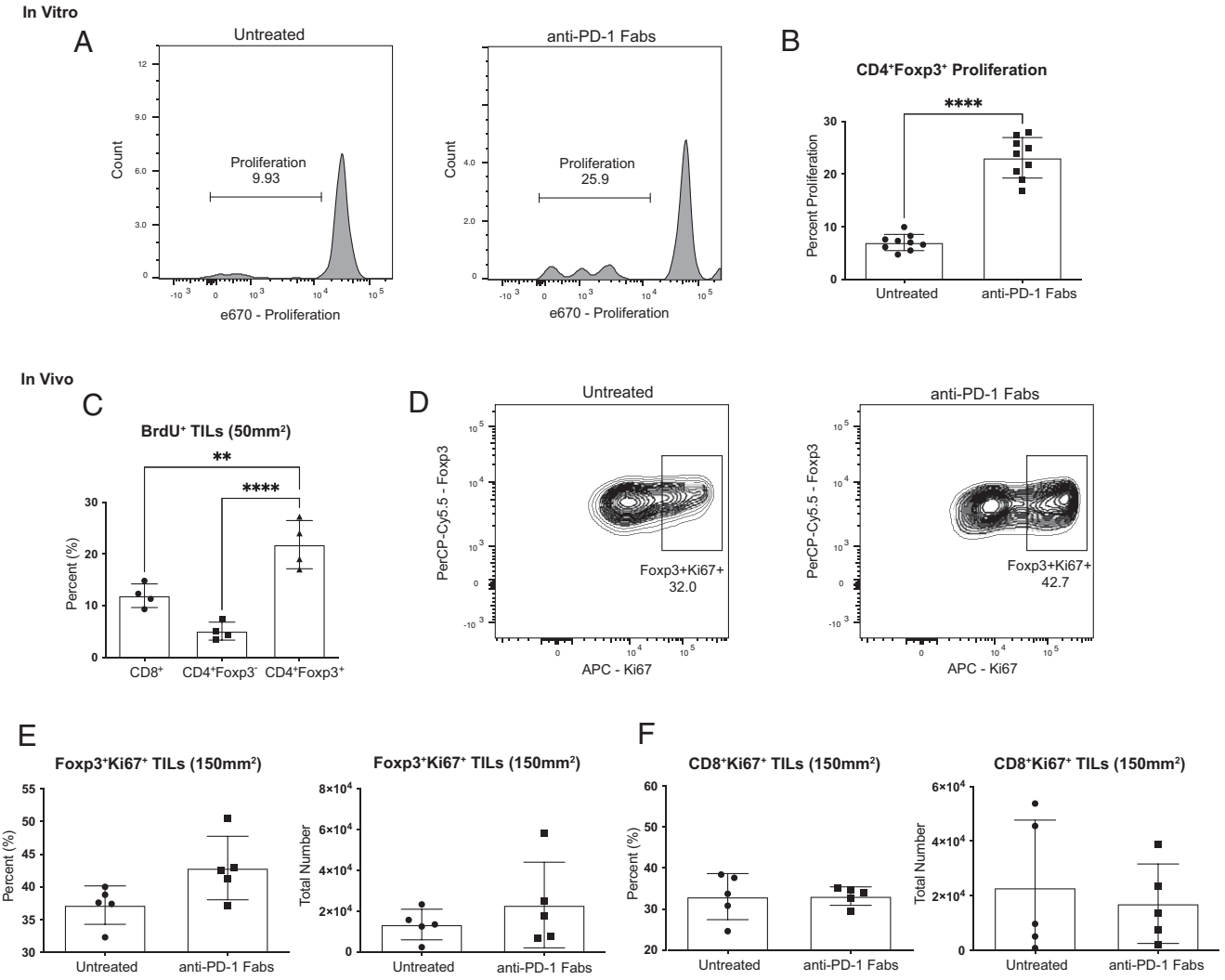

FIGURE 3. PD-1 blockade increases T_{reg} proliferation. Mice were injected with 1×10^4 T11 (claudin-low) tumor cells. (**A** and **B**) Tumors were harvested at 150 mm^2, digested, and enriched for lymphocytes, and GFP^+ T_{regs} were sorted using MoFlo-XDP cell sorter. T_{regs} stained with proliferation dye were incubated with or without anti–PD-1 Fabs, irradiated APCs, and soluble anti-CD3 in culture for 72 h. Cells were gated on lymphocytes/single cells/live/$Thy1.1^-/Foxp3^+$ and then analyzed for proliferation using e670 proliferation dye. (A) Representative flow plots gated on proliferation of T_{regs} cultured without or with anti–PD-1 Fabs (n = 9). (B) Percent proliferating $CD4^+Foxp3^+$ T_{regs} from in vitro culture. (**C**) Mice were injected with anti–PD-1 Ab and 2 mg BrdU. Tumors were harvested at 50 mm^2, digested, enriched for lymphocytes, and measured for BrdU incorporation by flow cytometry (n = 4). (**D**–**F**) Tumors were harvested at 150 mm^2 and enriched for lymphocytes, and Ki67 expression in $CD4^+Foxp3^+$ T_{regs} or $CD8^+$ T cells analyzed by FACS (n = 5). Cells were gated on lymphocytes/single cells/live/$CD45^+/CD4^+Foxp3^+$ or $CD8^+$, where indicated. Statistical significance determined by Mann–Whitney U test. $^{**}p < 0.01$, $^{****}p < 0.0001$.

TME is nonspecific and may contribute to the lack of synergy using ABT-199 with checkpoint inhibitors.

Higher levels of Foxp3 expression have been associated with increased suppressive capabilities in T_{regs} (29). Elevated levels of Foxp3 in T_{regs} treated with PD-1 blockade described earlier (Fig. 1E) prompted us to examine whether T_{regs} treated with PD-1 blockade had increased suppressive capabilities. We interrogated several pathways that could be used by T_{regs} to suppress antitumor immune responses in the TME from T11 (claudin-low)-bearing mice with or without PD-1 blockade. Expression of the inhibitory receptor CTLA-4, the high-affinity IL-2 receptor chain CD25, secretion of the suppressive cytokine TGF-β, and expression of GITR are well characterized either as mechanisms of suppression used by T_{regs} (34, 35) or characteristic of T_{reg} function (CD25) in limiting the availability of IL-2. All of these are known to contribute to their suppressive capabilities (36). After PD-1 blockade, there was an increase in the mean frequency of T_{regs} expressing suppressive markers CTLA-4, GITR, and TGF-β ($p = 0.09$, $p = 0.05$, and $p = 0.07$, respectively), with only the difference in GITR meeting the predefined definition of statistical significance for these studies (Fig. 6A). There were no significant differences in the level of expression of these molecules in T_{regs} as determined by the MFI (Fig. 6B). We wanted to confirm our findings in an additional model of claudin-low breast cancer (T12) that we have previously demonstrated to be enriched in T_{regs} and refractory to PD-1 blockade therapy (23). After PD-1 blockade in the T12 (claudin-low) model, there was an increase in the mean frequency of T_{regs} expressing GITR and TGF-β (Supplemental Fig. 4A). There was no difference in CD25 expression on T_{regs} from mice treated with PD-1 blockade, but the MFI of CD25 was increased on T_{regs} after PD-1 blockade (Supplemental Fig. 4B). Based on these findings, we then sought to test whether T_{regs} exposed to PD-1 blockade had increased suppressive capabilities. To address this, we treated Foxp3-GFP T11 (claudin-low) tumor-bearing mice with anti–PD-1 or left them untreated, and the tumors were harvested around 150 mm^2 for isolation of TILs. T_{regs} that had been exposed in the TME to PD-1 blockade were significantly better at suppressing naive $CD8^+$ T cell proliferation in an ex vivo setting than T_{regs} from mice that were untreated (Fig. 6C). These differences in suppression were

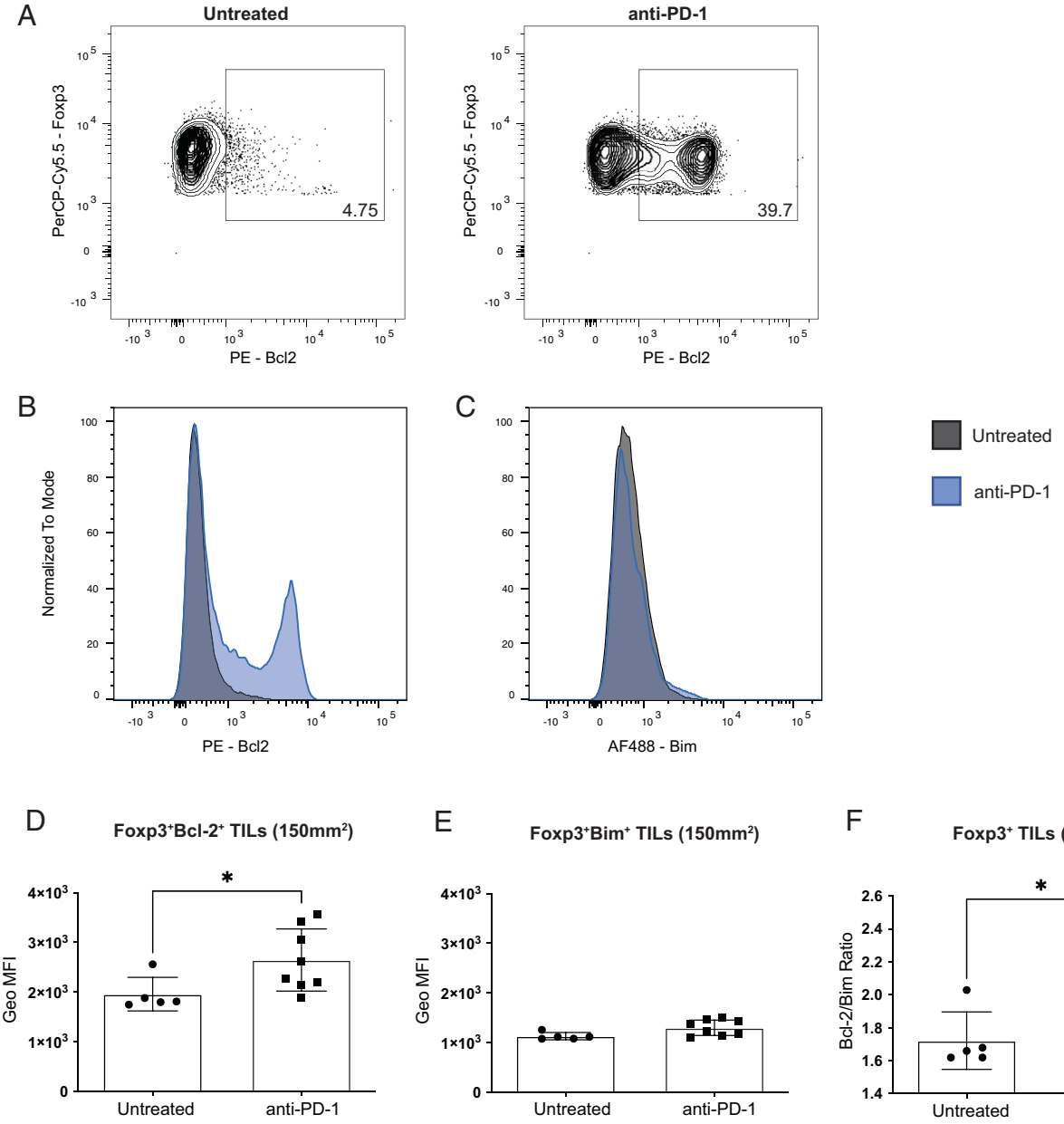

FIGURE 4. T_{regs} exposed to PD-1 blockade have increased Bcl-2 expression. BALB/c mice were injected with 1×10^4 T11 (claudin-low) tumor cells. Mice were untreated or treated with 200 μg anti–PD-1 Ab (J43) injected i.p. twice a week for the duration of the experiment. Tumors were harvested at 150 mm^2, digested, enriched for lymphocytes, and analyzed by FACS. Cells were gated on lymphocytes/single cells/live/$CD45^+$/$Foxp3^+$ from tumors of mice without or with anti–PD-1 treatment. (**A**) Representative flow plots showing frequency of $Bcl2^+$ cells of $CD4^+Foxp3^+$ ($n = 9$). (**B** and **C**) Histogram overlays of Bcl2 and Bim expression in $CD4^+Foxp3^+$ ($n = 9$). (**D**) Geometric (Geo) MFI of Bcl-2 in $CD4^+Foxp3^+$ cells in untreated compared with mice treated with anti–PD-1 ($n = 5$ untreated; $n = 8$ anti–PD-1). (**E**) MFI of Bim in $CD4^+Foxp3^+$ cells in untreated compared with mice treated with anti–PD-1 ($n = 5$ untreated; $n = 8$ anti–PD-1). (**F**) Ratio of Bcl-2 to Bim MFIs from (D) and (E) in $CD4^+Foxp3^+$ cells ($n = 5$ untreated; $n = 8$ anti–PD-1). Statistical significance determined by Mann–Whitney U test. $*p < 0.05$. AF, Alexa Fluor.

significant at a 2:1 ($p = 0.005$) and a 1:1 ($p = 0.02$) ratio of T_{regs} to $CD8^+$ T cells (Fig. 6C). Based on our previous work, the ratio of T_{regs} to $CD8^+$ T cells in the T11 (claudin-low) TME is ∼1.5:1 (23); thus, the suppressive effect observed in our experiment is biologically relevant to T_{reg}-dependent inhibition of conventional T cell activation at the ratios used in vitro.

Discussion

TNBC has the worst prognosis of the breast cancer subtypes despite being heavily immune infiltrated (37). The standard dogma in cancer immunotherapy is that tumors with immune infiltration have the capacity to mount a productive antitumor immune response and are therefore good candidates for immune checkpoint blockade. However, PD-1 is not only expressed on $CD8^+$ cytotoxic T lymphocytes but also on different populations of $CD4^+$ T and NK cells. Here, we show in a murine model that faithfully reproduces tumors found in patients with claudin-low breast cancer that PD-1 is most frequently expressed on $Foxp3^+$ T_{regs}. Blockade of PD-1 was associated with enhanced suppression, increased proliferation, and diminished apoptosis of T_{regs} in vitro, which was also reproduced in the TME. These data suggest that the activity of checkpoint

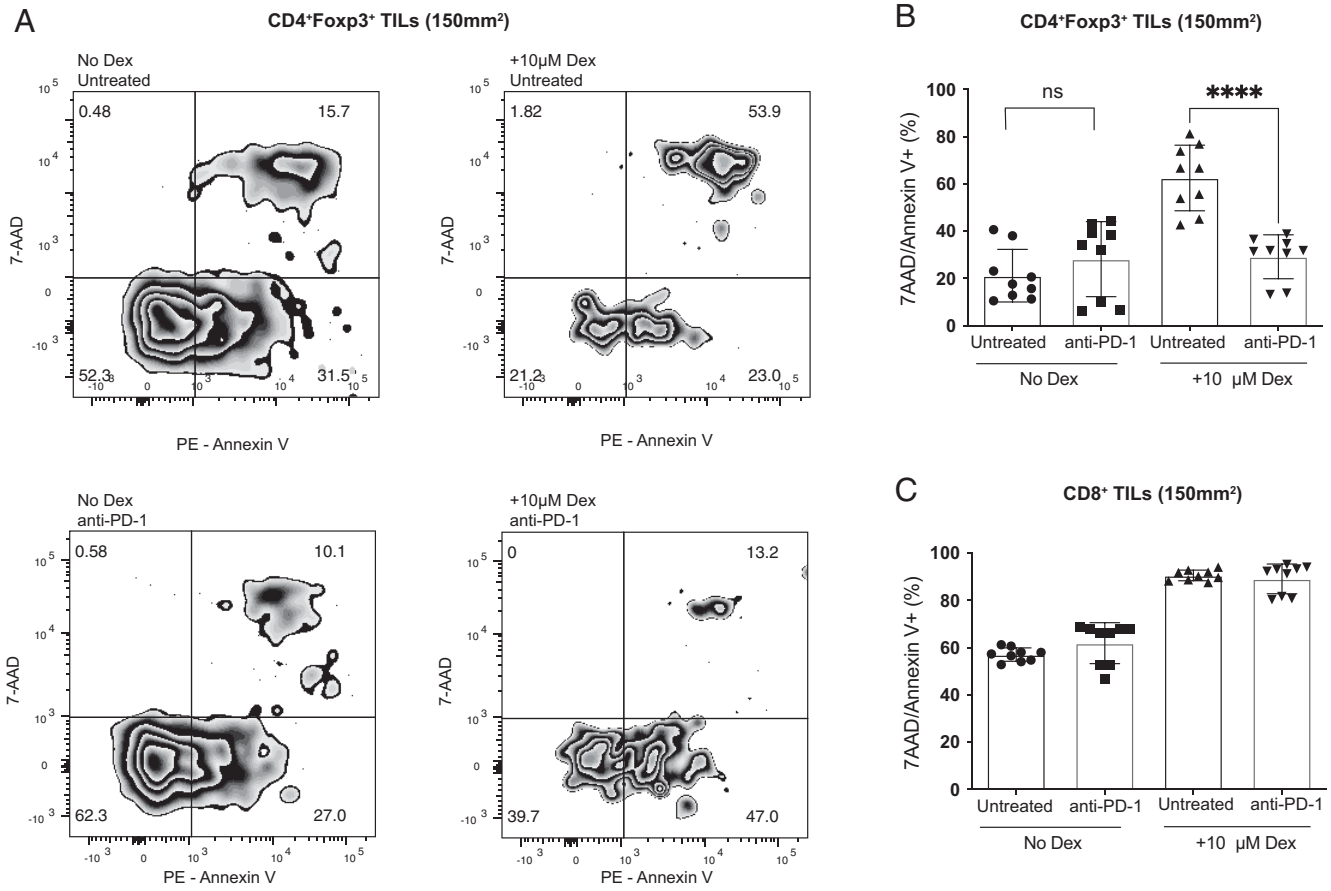

FIGURE 5. T_{regs} are protected from apoptosis after PD-1 blockade. BALB/c Foxp3-GFP mice were injected with 1×10^4 T11 (claudin-low) tumor cells. Mice were untreated or treated with 200 μg anti–PD-1 Ab (J43) injected i.p. twice a week for the duration of the experiment. Tumors were harvested at 150 mm^2, digested, and enriched for lymphocytes, and total T cells were isolated using cell isolation column ($n = 9$). Isolated total T cells were cultured in a 96-well plate in complete media or complete media + 10 μM Dex. Apoptosis was measured using Annexin V and 7-AAD staining. (**A**) Representative flow plots gated on GFP^+ T_{regs} isolated from the tumor of mice either untreated or treated with anti–PD-1 cultured with or without Dex. (**B**) Percent $CD4^+Foxp3^+$7-AAD/Annexin V^+ T_{regs} from $CD45^+$ parent population. (**C**) Percent $CD8^+$/7-AAD/Annexin V^+ T cells from $CD45^+$ parent population. Statistical significance was determined by Mann–Whitney U test. $^{****}p < 0.0001$.

inhibitors is more complicated than currently evaluated. The presence of a substantial immune infiltrate may not predict a response to immune checkpoint therapy if a significant number of the immune cells that express PD-1 are T_{regs}, which behave differently from conventional T cells on checkpoint inhibition.

The mechanism(s) for the enhanced function of T_{regs} in the presence of anti–PD-1 mAb therapy is not currently clear. Our data indicate that anti–PD-1 therapy affects at least three different pathways for T_{reg} activity. First, we found increased proliferation of T_{regs} in the presence of anti–PD-1 mAb therapy. This is consistent with findings evaluating the effects of anti–PD-1 mAb on the proliferation of $CD8^+$ T cells (11) and could be related to the increased expression of Jun and Fos in T_{regs} from anti–PD-1–treated animals. The second pathway is increased resistance to apoptosis. Previous work has demonstrated a critical role for the expression of Bcl family member proteins and decreased expression of Bim in the maintenance of T_{regs} (38). We found that anti–PD-1 therapy enhanced Bcl-2 expression and diminished GC-induced apoptosis in T_{regs}. Interestingly, we found that the Bcl-2 inhibitor ABT-199 could improve the median time for tumor growth in mice receiving T11 tumors, which was independent of coadministration with anti–PD-1 therapy. Given the extremely modest activity of ABT-199 in vitro against T11 tumor cells, these data suggest that inhibition of Bcl-2 in T11 tumors may also be because of diminished function of T_{regs}. Finally, T_{regs} exposed to anti–PD-1 therapy had enhanced suppressive function, which correlates with the increased expression of Foxp3 by those cells.

There are currently multiple ongoing clinical trials in TNBC where pembrolizumab (humanized anti–PD-1 Ab) is being given as a monotherapy (39). In all reported trials to date, the overall response rate to PD-1 inhibition in TNBC is reported to be between 4 and 20%, with only a small fraction of patients seeing any benefit from therapy (40). Our previous work has suggested that immune infiltration alone is not a reliable biomarker to predict overall response rate to immune checkpoint therapy, but instead the complete microenvironment including immunosuppression in the TME should be considered (23). Although the expected outcome of PD-1 therapy is that the inhibitory signal on cytotoxic T cells will be blocked, thereby allowing them to remain functional and lead to tumor killing, it is unknown whether PD-1 blockade functions similarly on other immune cell subsets that express PD-1. It has been hypothesized that therapeutic benefit from immune checkpoint blockade could be masked because of enhanced immunosuppression in the TME, leading to hyperprogression of cancer (14–16). Our study supports this hypothesis by demonstrating that PD-1 blockade promoted a prosurvival phenotype and enhanced suppression from $PD\text{-}1^+$ T_{regs} in the TME.

Most of the previous studies looking at the role of PD-1 on T_{regs} have been in vitro studies from peripheral T_{regs}. These studies broadly demonstrate that T_{regs} cultured in vitro with PD-1 blocking Ab enhance proliferation of T_{regs} (14, 17, 41, 42), although these

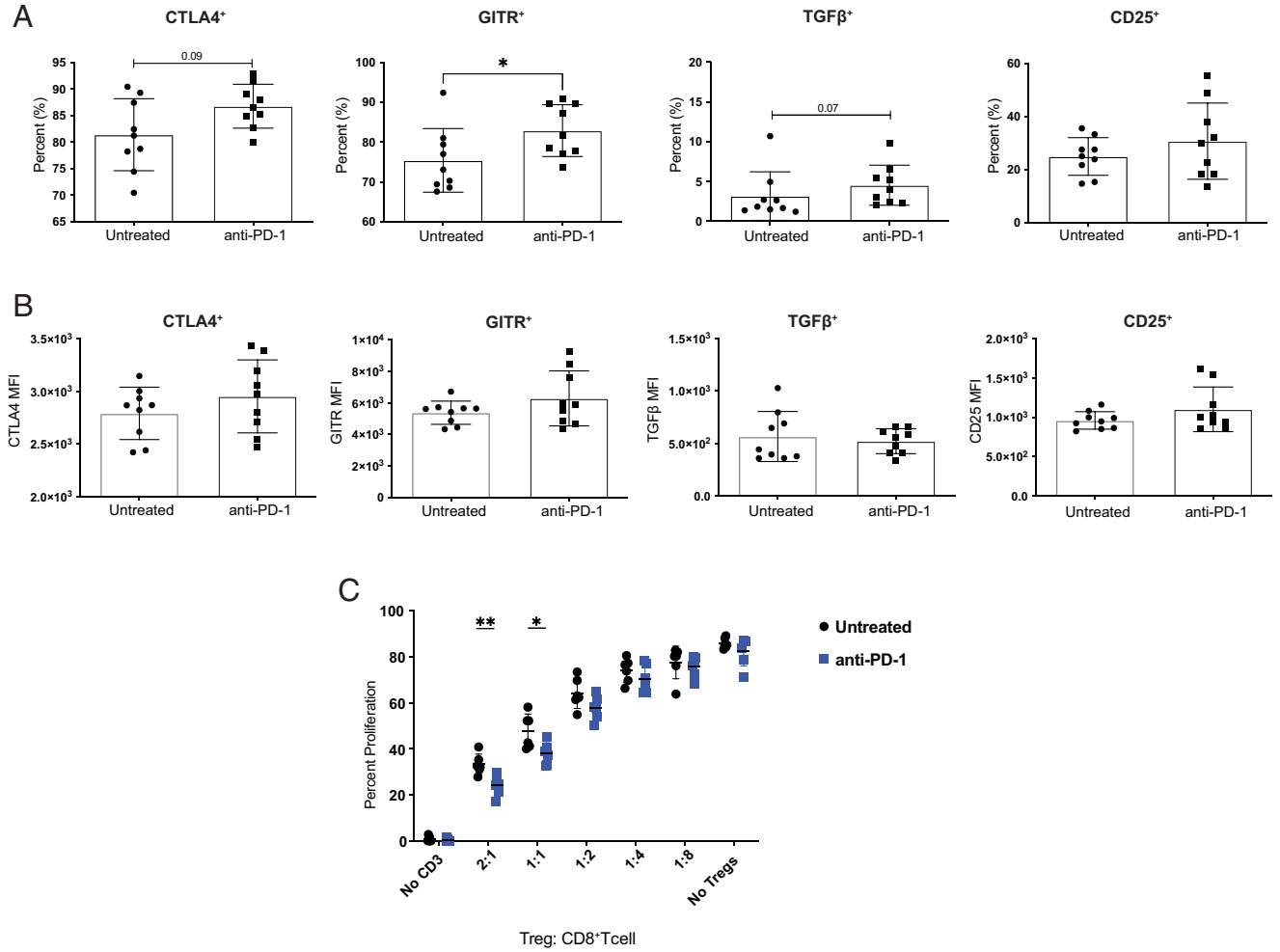

FIGURE 6. PD-1 blockade results in increased suppressive capabilities in T_{regs}. Mice were injected with 1×10^4 T11 (claudin-low) tumor cells. Mice were untreated or treated with 200 μg anti–PD-1 Ab (J43) injected i.p. twice a week for the duration of the experiment. (**A** and **B**) Tumors were harvested at 150 mm^2, digested, enriched for lymphocytes, and analyzed by FACS. Cells were gated on lymphocytes/single cells/live/$CD3^+$/$CD4^+Foxp3^+$ and then analyzed for T_{reg} markers. (A) Percent $CD4^+Foxp3^+$ T_{regs} expressing suppressive molecules; CTLA-4, GITR, TGF-β, and CD25 from mice treated with anti–PD-1 versus untreated ($n = 9$). (B) Geometric MFI of suppressive molecules in $CD4^+Foxp3^+$ cells ($n = 9$). Statistical significance determined by Mann–Whitney *U* test. (**C**) Tumors were harvested at 150 mm^2, digested, and enriched for lymphocytes, and GFP^+ T_{regs} were sorted using MoFlo-XDP cell sorter. Naive T cells were stained with proliferation dye and were incubated with sorted T_{regs}, irradiated APCs, and soluble anti–CD3 in culture for 72 h. Statistical significance was determined by multiple *t* tests. $*p < 0.05$, $**p < 0.01$.

studies are limited by the fact that T_{reg} function and proliferation were measured from peripheral T_{regs} rather than tissue-infiltrating T_{regs}. Our study is novel in that we directly measure the proliferative capacity and suppressive function of tumor-infiltrating T_{regs} treated with PD-1 blockade in vivo.

It was somewhat unexpected that the number of significantly expressed genes on T_{regs} in mice treated with or without anti–PD-1 mAb was quite modest. The evaluation of persistent expression of PD-1 on T cell exhaustion in vitro is difficult, and as a consequence, we chose to perform our screen using T_{regs} isolated from mice after in vivo treatment with anti–PD-1 mAb or control. One limitation to this approach was the performance of bulk RNA-seq on T_{regs} sorted from tumors, only 50% of which express PD-1 (Fig. 1B). Inclusion of PD-1-negative T_{regs} in our gene expression data may have minimized any changes to transcript regulation of T_{regs} from anti–PD-1 therapy. Furthermore, we could not assume that all PD-1–expressing T_{regs} would be exposed to saturating amounts of the Ab. Additional factors that might limit changes in gene expression could be a result of the timing of the administration of the Ab in relationship to the time of the RNA-seq evaluation. Nonetheless, we confirmed our findings by measuring protein expression of the relevant genes, thus allowing us to evaluate pathways that could mediate changes in T_{reg} function in the presence of anti–PD-1 mAb therapy.

In summary, we have shown in claudin-low tumors that T_{regs} express significant levels of PD-1. Blockade of PD-1 on these cells by anti–PD-1 therapy leads to enhanced T_{reg} proliferation, suppressive function, and resistance to apoptosis. The increased proliferation we observe is accompanied by increased expression of *Jun* and *Fos*, while the resistance to apoptosis is associated with increased expression of *Bcl-2*. These studies suggest that the activity and toxicity of checkpoint inhibitor therapy may be correlated with differences in expression of PD-1 on $CD8^+$ versus T_{regs}. We demonstrate in this study a model of breast cancer refractory to checkpoint inhibition that can be used to determine mechanistically how $PD\text{-}1^{high}$ T_{regs} in the TME alter outcomes to immunotherapy. This hypothesis should be tested clinically and specifically evaluated in the treatment of patients with TNBC, especially those of the claudin-low/mesenchymal subtype.

Acknowledgments

We acknowledge the University of North Carolina Flow Cytometry Core Facility for assistance in sorting and the high-throughput sequencing facility that sequenced samples.

Disclosures

C.M.P. is an equity stockholder and consultant of BioClassifier LLC; C.M.P. is also listed as an inventor on patent applications on the Breast PAM50 and Lung Cancer Subtyping assays. J.S.S. is an inventor on patent applications on Lung Cancer Subtyping assays, the use of innate lymphoid cells to treat graft-versus-host disease, and the use of STING agonists to enhance chimeric Ag receptor T cell therapy. The other authors have no financial conflicts of interest.

References

1. American Cancer Society. 2019. *Cancer Facts & Figures*. American Cancer Society, Atlanta, GA. Available at: https://www.cancer.org/content/dam/cancer-org/research/cancer-facts-and-statistics/annual-cancer-facts-and-figures/2019/cancer-facts-and-figures-2019.pdf.
2. Susan G. Komen. *Breast Cancer Fact Sheet*. Available at: https://ww5.komen.org/uploadedFiles/_Komen/Content/About_Breast_Cancer/Facts_and_Statistics/Breast_Cancer_in_Women/BCFactSheetOct2017.pdf. Accessed July 2019.
3. Bianchini, G., J. M. Balko, I. A. Mayer, M. E. Sanders, and L. Gianni. 2016. Triple-negative breast cancer: challenges and opportunities of a heterogeneous disease. *Nat. Rev. Clin. Oncol.* 13: 674–690.
4. Purrington, K. S., D. W. Visscher, C. Wang, D. Yannoukakos, U. Hamann, H. Nevanlinna, A. Cox, G. G. Giles, J. E. Eckel-Passow, S. Lakis, et al.; Jane Carpenter for ABCTC Investigators. 2016. Genes associated with histopathologic features of triple negative breast tumors predict molecular subtypes. *Breast Cancer Res. Treat.* 157: 117–131.
5. Prat, A., B. Adamo, M. C. Cheang, C. K. Anders, L. A. Carey, and C. M. Perou. 2013. Molecular characterization of basal-like and non-basal-like triple-negative breast cancer. *Oncologist* 18: 123–133.
6. Iglesia, M. D., J. S. Parker, K. A. Hoadley, J. S. Serody, C. M. Perou, and B. G. Vincent. 2016. Genomic Analysis of Immune Cell Infiltrates Across 11 Tumor Types. *J. Natl. Cancer Inst.* 108: djw144.
7. Lee, P. P., C. Yee, P. A. Savage, L. Fong, D. Brockstedt, J. S. Weber, D. Johnson, S. Swetter, J. Thompson, P. D. Greenberg, et al. 1999. Characterization of circulating T cells specific for tumor-associated antigens in melanoma patients. *Nat. Med.* 5: 677–685.
8. Pardoll, D. M. 2012. The blockade of immune checkpoints in cancer immunotherapy. *Nat. Rev. Cancer* 12: 252–264.
9. Wherry, E. J. 2011. T cell exhaustion. *Nat. Immunol.* 12: 492–499.
10. Wherry, E. J., J. N. Blattman, K. Murali-Krishna, R. van der Most, and R. Ahmed. 2003. Viral persistence alters CD8 T-cell immunodominance and tissue distribution and results in distinct stages of functional impairment. *J. Virol.* 77: 4911–4927.
11. Barber, D. L., E. J. Wherry, D. Masopust, B. Zhu, J. P. Allison, A. H. Sharpe, G. J. Freeman, and R. Ahmed. 2006. Restoring function in exhausted CD8 T cells during chronic viral infection. *Nature* 439: 682–687.
12. Iglesia, M. D., B. G. Vincent, J. S. Parker, K. A. Hoadley, L. A. Carey, C. M. Perou, and J. S. Serody. 2014. Prognostic B-cell signatures using mRNA-seq in patients with subtype-specific breast and ovarian cancer. *Clin. Cancer Res.* 20: 3818–3829.
13. Schmid, P., S. Adams, H. S. Rugo, A. Schneeweiss, C. H. Barrios, H. Iwata, V. Diéras, R. Hegg, S. A. Im, G. Shaw Wright, et al.; IMpassion130 Trial Investigators. 2018. Atezolizumab and Nab-Paclitaxel in Advanced Triple-Negative Breast Cancer. *N. Engl. J. Med.* 379: 2108–2121.
14. Kamada, T., Y. Togashi, C. Tay, D. Ha, A. Sasaki, Y. Nakamura, E. Sato, S. Fukuoka, Y. Tada, A. Tanaka, et al. 2019. PD-1^{+} regulatory T cells amplified by PD-1 blockade promote hyperprogression of cancer. *Proc. Natl. Acad. Sci. USA* 116: 9999–10008.
15. Ferrara, R., L. Mezquita, M. Texier, J. Lahmar, C. Audigier-Valette, L. Tessonnier, J. Mazieres, G. Zalcman, S. Brosseau, S. Le Moulec, et al. 2018. Hyperprogressive Disease in Patients With Advanced Non-Small Cell Lung Cancer Treated With PD-1/PD-L1 Inhibitors or With Single-Agent Chemotherapy. *JAMA Oncol.* 4: 1543–1552.
16. Kim, C. G., K. H. Kim, K. H. Pyo, C. F. Xin, M. H. Hong, B. C. Ahn, Y. Kim, S. J. Choi, H. I. Yoon, J. G. Lee, et al. 2019. Hyperprogressive disease during PD-1/PD-L1 blockade in patients with non-small-cell lung cancer. *Ann. Oncol.* 30: 1104–1113.
17. Woods, D. M., R. Ramakrishnan, A. S. Laino, A. Berglund, K. Walton, B. C. Betts, and J. S. Weber. 2018. Decreased suppression and increased phosphorylated STAT3 in regulatory T cells are associated with benefit from adjuvant PD-1 blockade in resected metastatic melanoma. *Clin. Cancer Res.* 24: 6236–6247.
18. Dodagatta-Marri, E., D. S. Meyer, M. Q. Reeves, R. Paniagua, M. D. To, M. Binnewies, M. L. Broz, H. Mori, D. Wu, M. Adoumie, et al. 2019. α-PD-1 therapy elevates Treg/Th balance and increases tumor cell pSmad3 that are both targeted by α-TGFβ antibody to promote durable rejection and immunity in squamous cell carcinomas. *J. Immunother. Cancer* 7: 62.
19. Hsu, J., J. J. Hodgins, M. Marathe, C. J. Nicolai, M. C. Bourgeois-Daigneault, T. N. Trevino, C. S. Azimi, A. K. Scheer, H. E. Randolph, T. W. Thompson, et al. 2018. Contribution of NK cells to immunotherapy mediated by PD-1/PD-L1 blockade. *J. Clin. Invest.* 128: 4654–4668.
20. Quatrini, L., E. Wieduwild, B. Escaliere, J. Filtjens, L. Chasson, C. Laprie, E. Vivier, and S. Ugolini. 2018. Endogenous glucocorticoids control host resistance to viral infection through the tissue-specific regulation of PD-1 expression on NK cells. *Nat. Immunol.* 19: 954–962.
21. Yu, Y., J. C. Tsang, C. Wang, S. Clare, J. Wang, X. Chen, C. Brandt, L. Kane, L. S. Campos, L. Lu, et al. 2016. Single-cell RNA-seq identifies a PD-1^{hi} ILC progenitor and defines its development pathway. *Nature* 539: 102–106.
22. Shi, J., S. Hou, Q. Fang, X. Liu, X. Liu, and H. Qi. 2018. PD-1 Controls Follicular T Helper Cell Positioning and Function. *Immunity* 49: 264–274.e4.
23. Taylor, N. A., S. C. Vick, M. D. Iglesia, W. J. Brickey, B. R. Midkiff, K. P. McKinnon, S. Reisdorf, C. K. Anders, L. A. Carey, J. S. Parker, et al. 2017. Treg depletion potentiates checkpoint inhibition in claudin-low breast cancer. *J. Clin. Invest.* 127: 3472–3483.
24. Gallimore, A., S. A. Quezada, and R. Roychoudhuri. 2019. Regulatory T cells in cancer: where are we now? *Immunology* 157: 187–189.
25. Usary, J., D. B. Darr, A. D. Pfefferle, and C. M. Perou. 2016. Overview of genetically engineered mouse models of distinct breast cancer subtypes. *Curr. Protoc. Pharmacol.* 72: 14.38.1–14.38.11.
26. Burgents, J. E., T. P. Moran, M. L. West, N. L. Davis, R. E. Johnston, and J. S. Serody. 2010. The immunosuppressive tumor environment is the major impediment to successful therapeutic vaccination in Neu transgenic mice. *J. Immunother.* 33: 482–491.
27. Love, M. I., W. Huber, and S. Anders. 2014. Moderated estimation of fold change and dispersion for RNA-seq data with DESeq2. *Genome Biol.* 15: 550.
28. Blackburn, S. D., H. Shin, G. J. Freeman, and E. J. Wherry. 2008. Selective expansion of a subset of exhausted CD8 T cells by alphaPD-L1 blockade. *Proc. Natl. Acad. Sci. USA* 105: 15016–15021.
29. Chauhan, S. K., D. R. Saban, H. K. Lee, and R. Dana. 2009. Levels of Foxp3 in regulatory T cells reflect their functional status in transplantation. *J. Immunol.* 182: 148–153.
30. Huen, N. Y., A. L. Pang, J. A. Tucker, T. L. Lee, M. Vergati, C. Jochems, C. Intrivici, V. Cereda, W. Y. Chan, O. M. Rennert, et al. 2013. Up-regulation of proliferative and migratory genes in regulatory T cells from patients with metastatic castration-resistant prostate cancer. *Int. J. Cancer* 133: 373–382.
31. Gerdes, J., U. Schwab, H. Lemke, and H. Stein. 1983. Production of a mouse monoclonal antibody reactive with a human nuclear antigen associated with cell proliferation. *Int. J. Cancer* 31: 13–20.
32. Vaux, D. L., S. Cory, and J. M. Adams. 1988. Bcl-2 gene promotes haemopoietic cell survival and cooperates with c-myc to immortalize pre-B cells. *Nature* 335: 440–442.
33. Souers, A. J., J. D. Leverson, E. R. Boghaert, S. L. Ackler, N. D. Catron, J. Chen, B. D. Dayton, H. Ding, S. H. Enschede, W. J. Fairbrother, et al. 2013. ABT-199, a potent and selective BCL-2 inhibitor, achieves antitumor activity while sparing platelets. *Nat. Med.* 19: 202–208.
34. Schmidt, A., N. Oberle, and P. H. Krammer. 2012. Molecular mechanisms of treg-mediated T cell suppression. *Front. Immunol.* 3: 51.
35. Shimizu, J., S. Yamazaki, T. Takahashi, Y. Ishida, and S. Sakaguchi. 2002. Stimulation of CD25(+)CD4(+) regulatory T cells through GITR breaks immunological self-tolerance. *Nat. Immunol.* 3: 135–142.
36. McHugh, R. S., M. J. Whitters, C. A. Piccirillo, D. A. Young, E. M. Shevach, M. Collins, and M. C. Byrne. 2002. CD4(+)CD25(+) immunoregulatory T cells: gene expression analysis reveals a functional role for the glucocorticoid-induced TNF receptor. *Immunity* 16: 311–323.
37. Waks, A. G., and E. P. Winer. 2019. Breast Cancer Treatment. *JAMA* 321: 316.
38. Tischner, D., I. Gaggl, I. Peschel, M. Kaufmann, S. Tuzlak, M. Drach, N. Thuille, A. Villunger, and G. Jan Wiegers. 2012. Defective cell death signalling along the Bcl-2 regulated apoptosis pathway compromises Treg cell development and limits their functionality in mice. *J. Autoimmun.* 38: 59–69.
39. Adams, S., P. Schmid, H. S. Rugo, E. P. Winer, D. Loirat, A. Awada, D. W. Cescon, H. Iwata, M. Campone, R. Nanda, et al. 2017. Phase 2 study of pembrolizumab (pembro) monotherapy for previously treated metastatic triple-negative breast cancer (mTNBC): KEYNOTE-086 cohort A. *J. Clin. Oncol.* 35(Suppl. 15): 1008.
40. Wein, L., S. J. Luen, P. Savas, R. Salgado, and S. Loi. 2018. Checkpoint blockade in the treatment of breast cancer: current status and future directions. *Br. J. Cancer* 119: 4–11.
41. Franceschini, D., M. Paroli, V. Francavilla, M. Videtta, S. Morrone, G. Labbadia, A. Cerino, M. U. Mondelli, and V. Barnaba. 2009. PD-L1 negatively regulates CD4+CD25+Foxp3+ Tregs by limiting STAT-5 phosphorylation in patients chronically infected with HCV. *J. Clin. Invest.* 119: 551–564.
42. Wong, M., A. La Cava, and B. H. Hahn. 2013. Blockade of programmed death-1 in young (New Zealand Black x New Zealand White)F1 mice promotes the suppressive capacity of CD4+ regulatory T cells protecting from lupus-like disease. *J. Immunol.* 190: 5402–5410.

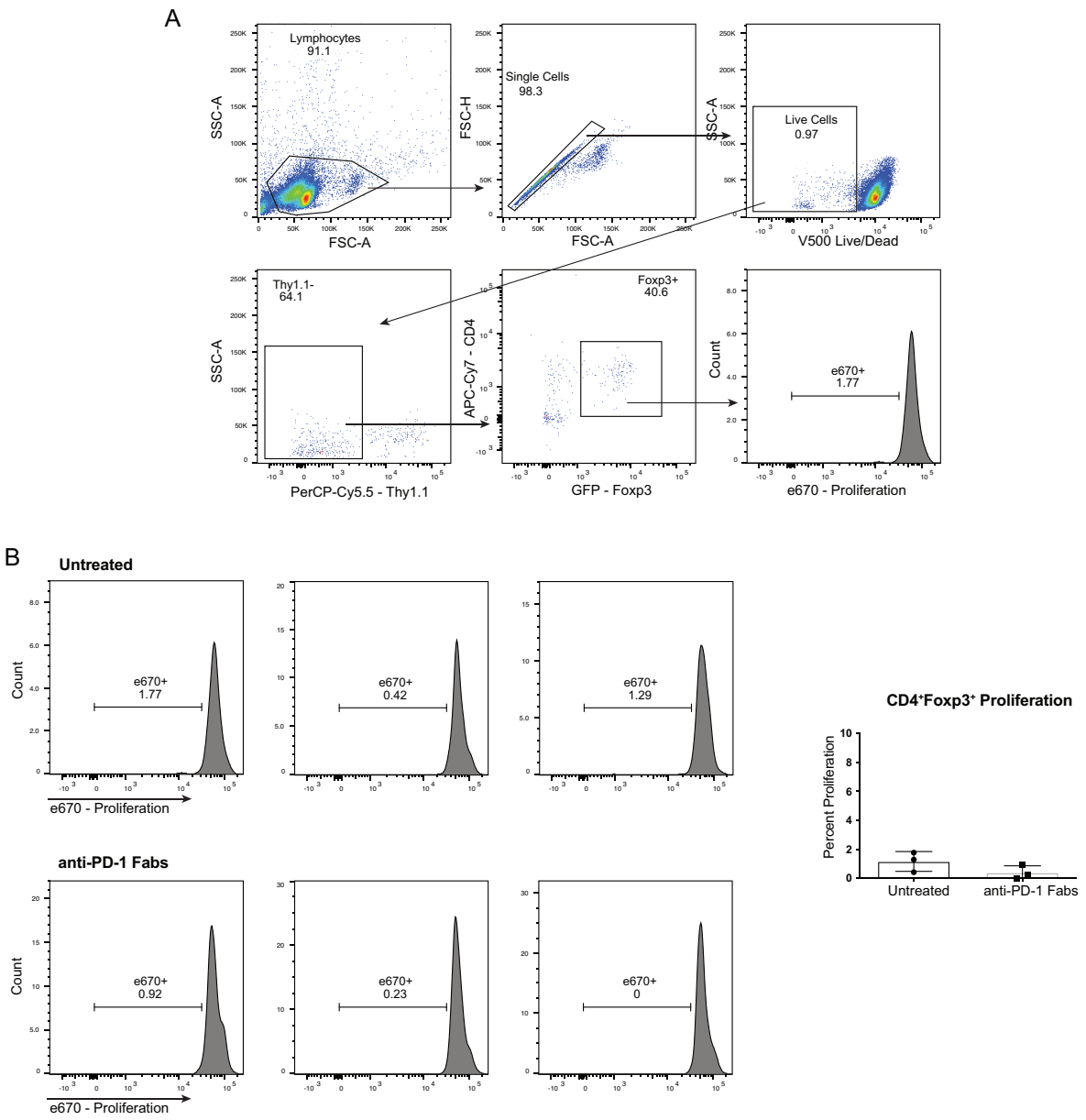

Supplementary Figure S1: PD-1 antibody alone does not result in T_{reg} proliferation. Mice were injected with 1 x 10^4 T11 (claudin-low) tumor cells. (**A-B**) Tumors were harvested at 150mm^2, digested, enriched for lymphocytes, and GFP+ T_{regs} were sorted using MoFlo-XDP cell sorter. T_{regs} stained with proliferation dye were incubated with or without α-PD-1 Fabs and irradiated APCs without α-CD3 in culture for 72 hours. (**A**) Flow cytometry gating strategy for proliferation of T_{regs} cultured without or with α-PD-1 Fabs. (n=3) (**B**) Percent proliferating $CD4^+Foxp3^+$ T_{regs} from in vitro culture.

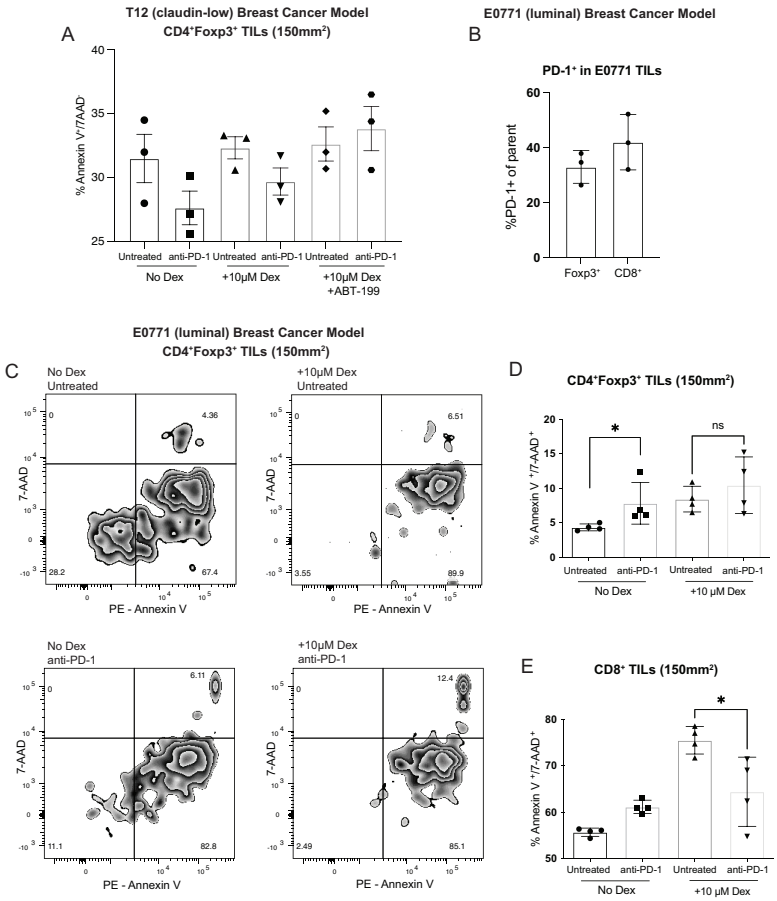

Supplementary Figure S2. Apoptosis of T_{regs} after PD-1 blockade in T12 (claudin-low) and E0771 (luminal) breast cancer models. **(A)** BALB/c Foxp3-GFP mice were injected with 1 x 10^5 T12 (claudin-low) tumor cells (n=3) or **(B-E)** B6 Foxp3-GFP mice were injected with 2.5x10^5 E0771 cells (n=4). Mice were untreated or treated with 200 μg α-PD-1 antibody (J43) injected IP twice a week for the duration of the experiment. Isolated total T cells were cultured in 96 well plate in complete media or complete media + 10μM Dexamethasone + 20μM ABT-199. Apoptosis was measured using Annexin V and 7-AAD staining. **(A)** Percent $CD4^+Foxp3^+$7-AAD/Annexin V^+ T_{regs}. **(B)** Percent PD-1^+ of T_{regs} or CD8 T cells among E0771 TILs. (**C**) Representative flow plots gated on GFP^+ T_{regs}. (**D**) Percent $CD4^+Foxp3^+$7-AAD/Annexin V^+ T_{regs} from $CD45^+$ parent population. (**E**) Percent $CD8^+$/7-AAD/Annexin V^+ T cells from $CD45^+$ parent population. Statistical significance determined by Mann-Whitney test. * denotes $p < 0.05$.

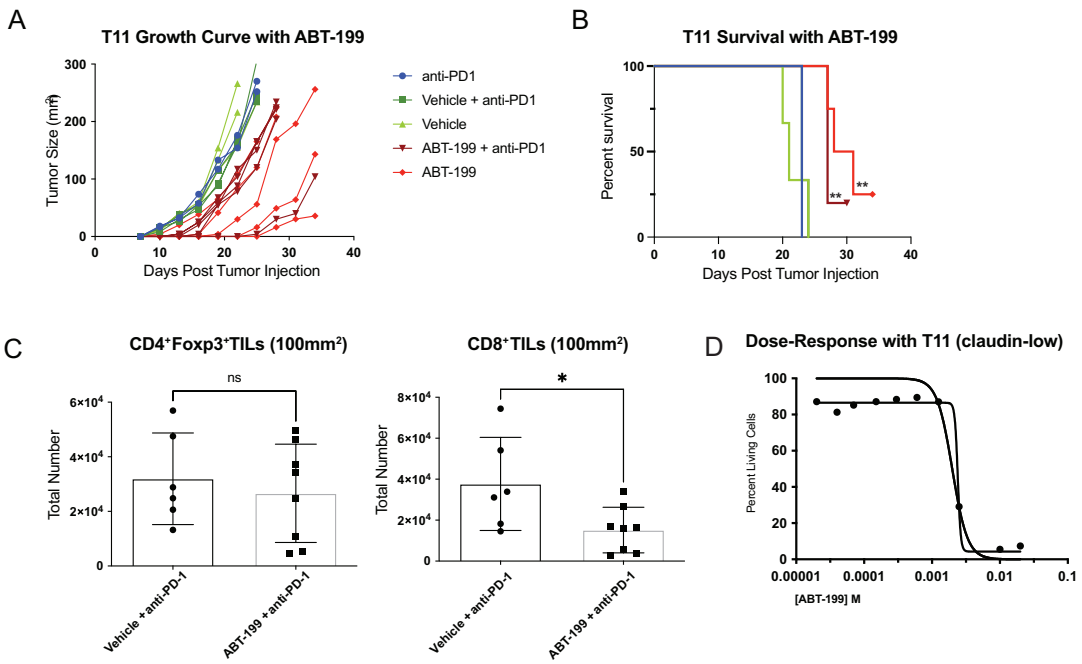

Supplementary Figure S3: Inhibition of Bcl-2 leads to delay of tumor growth and increase in survival. BALB/c mice were injected with 1 x 10^4 T11 (claudin-low) tumor cells. Mice were untreated or treated with 200µg α-PD-1 antibody (J43) injected IP twice a week for the duration of the experiment. Mice were also given ABT-199 (100mg/kg) daily, or vehicle daily by oral gavage from day +1 for the duration of the experiment. (**A**) Individual replicates of tumor growth curves. (**B**) Mice receiving Bcl-2 inhibitor ABT-199 and ABT-199 + α-PD-1 (n = 3) have a significant survival benefit compared to mice receiving vehicle (n=3) or α-PD-1 alone (n = 3) (p = 0.0046; log-rank test for Vehicle + α-PD-1 vs ABT-199 + α-PD-1) (p = 0.0042; log-rank test for Vehicle vs ABT-199). (**C**) Tumors were harvested at 100mm^2, digested, enriched for lymphocytes, and analyzed by FACS. (Vehicle + α-PD-1 n=6, ABT-199 + α-PD-1 n=8) (**C**) Total number of $CD4^+Foxp3^+$ T_{regs}. (**D**) T11 (claudin-low) tumor cells were plated in a 96 well plate at 1.5x10^4 cells/well and incubated for 24 hours at 37°C. ABT-199 was added at a starting concentration of 20µM and serially diluted. T11 cells plus ABT-199 were incubated at 37°C 5% CO2 for 48 hours. Cell death was measured using Sigma MTT Cell Growth Assay.

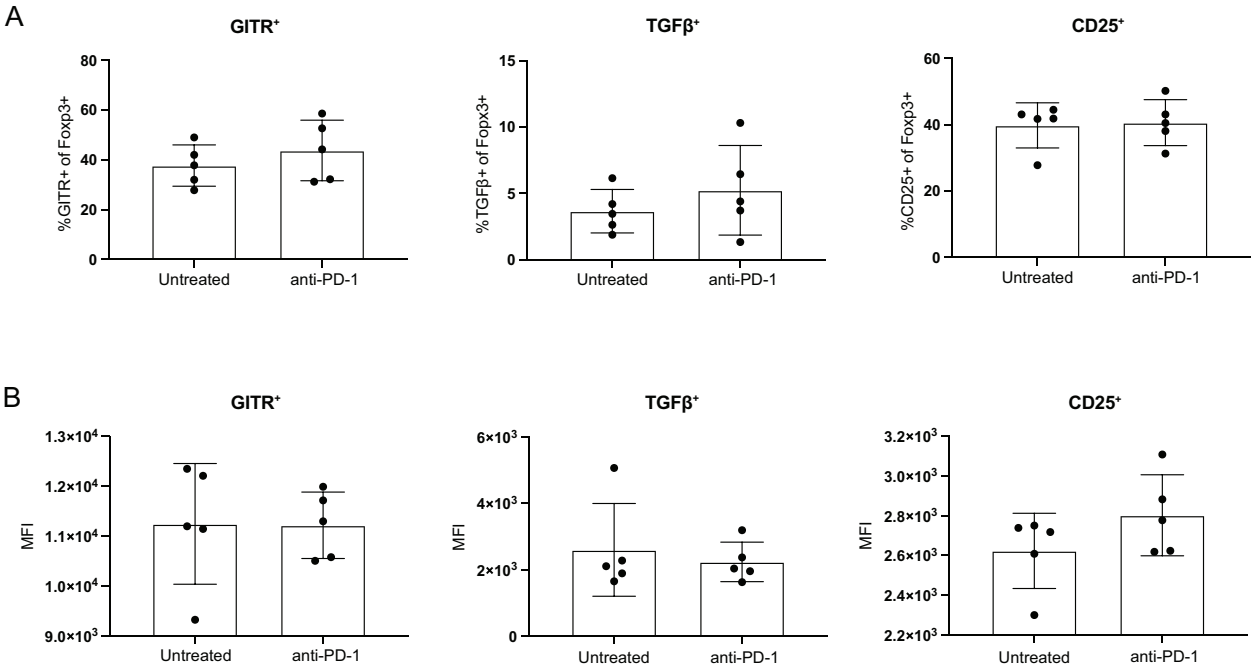

Supplementary Figure S4: Characterization of T_{regs} from T12 (claudin-low) tumor model. Mice were injected with 1 x 10^5 T12 (claudin-low) tumor cells in Matrigel low-growth factor. Mice were untreated or treated with 200 μg α-PD-1 antibody (J43) injected IP twice a week for the duration of the experiment. (**A-B**) Tumors were harvested at 150mm^2, digested, enriched for lymphocytes, and analyzed by FACS. (**A**) Percent $CD4^+Foxp3^+$ T_{regs} expressing suppressive molecules; GITR, TGFβ, and CD25 from mice treated with α-PD-1 versus untreated (n=5). (**B**) Geometric Mean Fluorescence Intensity of suppressive molecules in $CD4^+Foxp3^+$ cells (n=5). Statistical significance determined by Mann-Whitney test.